# D4.1– Report on ASR with the different chemical compositions and particle sizes measured at initial operation and after 3000 hours of aging

## PROJECT INFORMATION

| | |
|---|---|
| **GRANT AGREEMENT NUMBER** | 826323 |
| **PROJECT FULL TITLE** | Low Cost Interconnects with highly improved Contact Strength for SOC Applications |
| **PROJECT ACRONYM** | LOWCOST-IC |
| **FUNDING SCHEME** | FCH-JU2 |
| **START DATE OF THE PROJECT** | 1/1-2019 |
| **DURATION** | 36 months |
| **CALL IDENTIFIER** | H2020-JTI-FCH-2018-1 |
| **PROJECT WEBSITE** | www.lowcost-ic.eu |

## DELIVERABLE INFORMATION

| | |
|---|---|
| **WP NO.** | 4 |
| **WP LEADER** | Belma Talic |
| **CONTRIBUTING PARTNERS** | DTU |
| **NATURE** | Report |
| **AUTHORS** | Belma Talic |
| **CONTRIBUTORS** | |
| **CONTRACTUAL DEADLINE** | M12 – 31.12.2019 |
| **DELIVERY DATE TO EC** | 20.12-2019 |

DISSEMINATION LEVEL

| | | |
|---|---|---|
| PU | Public | X |
| PP | Restricted to other programme participants (incl. Commission Services) | |
| RE | Restricted to a group specified by the consortium (incl. Commission Services) | |
| CO | Confidential, only for the members of the consortium (incl. Commission Services) | |

# 1  Introduction

Stacking of solid oxide cells (SOC) requires that a robust and durable electrical contact between the cell and the interconnect is established. To achieve this, contact layers are applied during the cell fabrication process or the stack assembly. Perovskite oxides are commonly used as the contact material in current state-of-the-art SOC stacks due to their high electrical conductivity and good compatibility with the SOC oxygen electrode material. However, sintering of these materials requires a high temperature (> 1000C), which is not compatible with the other SOC stack components such as the steel interconnect and the glass(-ceramic) sealant. As a results of the poor sintering at lower temperature, the interface between the oxygen electrode and the interconnect is among the weakest in the stack and the one most prone to loss of contact.

In the LOWCOST-IC project, we have investigated a novel contact layer solution based on the concept of reactive oxidative bonding. In this method, the contact layer is applied in the form of metal particles that during SOC stack operation (700-800 °C) are oxidized *in-situ* to form dense and well-conducting oxides. The concept is illustrated in Figure 1. The metallic precursors investigated are Mn-Co and Mn-Cu, mixed in the stoichiometric ratios to form $MnCo_2O_4$ and $Cu_{1.3}Mn_{1.7}O_4$, respectively. The compositions were chosen as both oxides have an appreciable electrical conductivity (70 and 225 S/cm at 750 °C, respectively) and a TEC (14.4 and 12.2 $K^{-1}$ between 25 °C and 800 °C, respectively) matching other typically used SOC materials [1,2]. Due to the high reactivity of the metallic precursors, a strong bond is created to both the coated interconnect and the air electrode [3].

In order to validate this contact layer solution, the area specific resistance (ASR) has been measured over a stack element consisting of the coated interconnect, the contact layer material and an oxygen electrode.  The ASR is evaluated at 750°C and 850 °C, representing the average operating temperature for the stack of Solid Power and Sunfire, respectively. The chemical stability of the contact layer/interconnect interface is evaluated by post-test analysis by SEM and EDS.
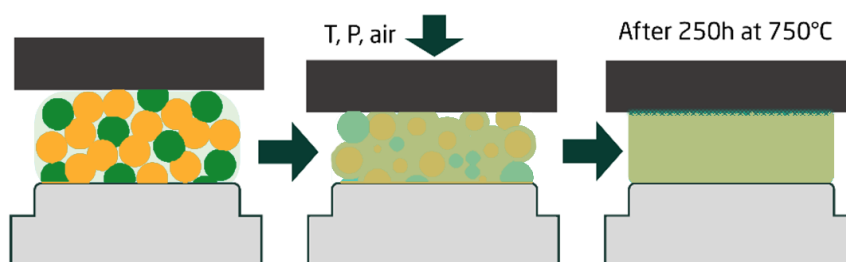


**Figure 1. Schematic illustration of the reactive oxidative bonding concept for fabrication of tougher contact layers**

# 2 Materials and methods

The area specific resistance (ASR) was measured at DTU using a well-established set-up described in detail in Ref. [4,5]. An illustration of a "single repeating unit" in this set-up is shown in Figure 2. By stacking several of these units together into a "stack" the ASR as a function of time can be measured across multiple interfaces simultaneously. The stacks used for the measurement at 750 °C and 850 °C are schematically illustrated in Figure 3.
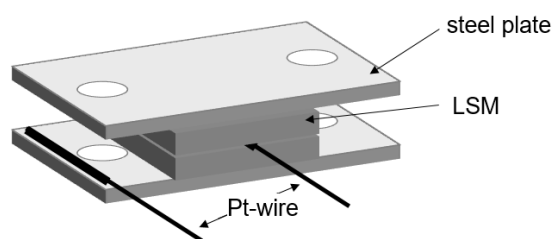


**Figure 2. Single repeating unit for the ASR measurement**

The ferritic stainless steel AISI 441 in 0.3 mm thickness served as the interconnect material. For the measurement at 750 °C, one side of the steel was coated with CeCo (Sandvik Materials – produced on the production line) while the other side was left uncoated. For the measurement at 850 °C, both side of the steel were coated with CeCo (Sandvik Materials – produced with batch coater). The steel was cut into 20x40 mm$^2$ coupons and a Pt wire was spot welded along one of the shorter edges, to act as a voltage probe. For the single-side coated steel, the Pt-wire was welded to the uncoated side, while for the dual-side coated steel, the Pt-wire was welded on top of the (metallic) Co-coating.

Two different contact layers, Mn-Co and Mn-Cu, were screen printed onto a 20x20 mm$^2$ central area of the interconnect with a green thickness of ca. 0.2 mm. The pastes for screen printing were prepared using Mn (American Elements, 99.9 %, APS ~ 2 µm), Co (Alfa Aesar, 99.8 %, APS ~ 1.6 µm) and Cu (Alfa Aesar, 99 %, APS ~ 2-3.5 µm) metal powders, and a proprietary solvent + binder system developed at DTU. The powders were added in the stoichiometric amounts to upon oxidation form $MnCo_2O_4$ and $Cu_{1.3}Mn_{1.7}O_4$, respectively. The paste was dried at 90 °C for 1 h after screen printing, to evaporate the solvent before assembly.

Bisque-sintered $La_{0.85}Sr_{0.1}Mn_{1.1}O_3$ (LSM) plates (20x20x1 mm$^3$) spray coated with a 50-60 µm layer of LSM and $Co_3O_4$ slurry mixture were used as the current collection plates. The LSM plates were stacked between the interconnect coupons as illustrated in Figures 2 and 3. Gold foil connected to gold wires was placed on the top and bottom of the stack to supply the current. A  load of 7 kg was put on top of the stack. The stack was heated in stagnant air following a representative SOC stack heat-up profile used when employing glass-ceramic sealants, see reference (11). This involved heating to 600 °C at 100 °C/h, holding for 1 h, heating to 700 °C at 100 °C/h, heating to 800 °C at 50 °C/h, holding for 1 h and finally cooling/heating (at 120 °C/h) to the operating temperature of 750 °C or 850 °C . At 750/850 °C, a measurement current of 2 A was employed, corresponding to

0.5 A/cm$^2$ considering the nominal contact area between the steel interconnect and the LSM plate.

The ASR was calculated according to Ohm's law, by measuring the voltage drop between the Pt-wire connected to the interconnect and a Pt-wire placed between two LSM plates:

$$ASR = \frac{\Delta V}{I} \cdot A$$

where ΔV is the voltage drop, I is the current and A is the nominal contact area.

The cross-plane resistance (ASR) was measured across seven different configurations at 750 °C and four different configurations at 850 °C, summarized in Table 1.
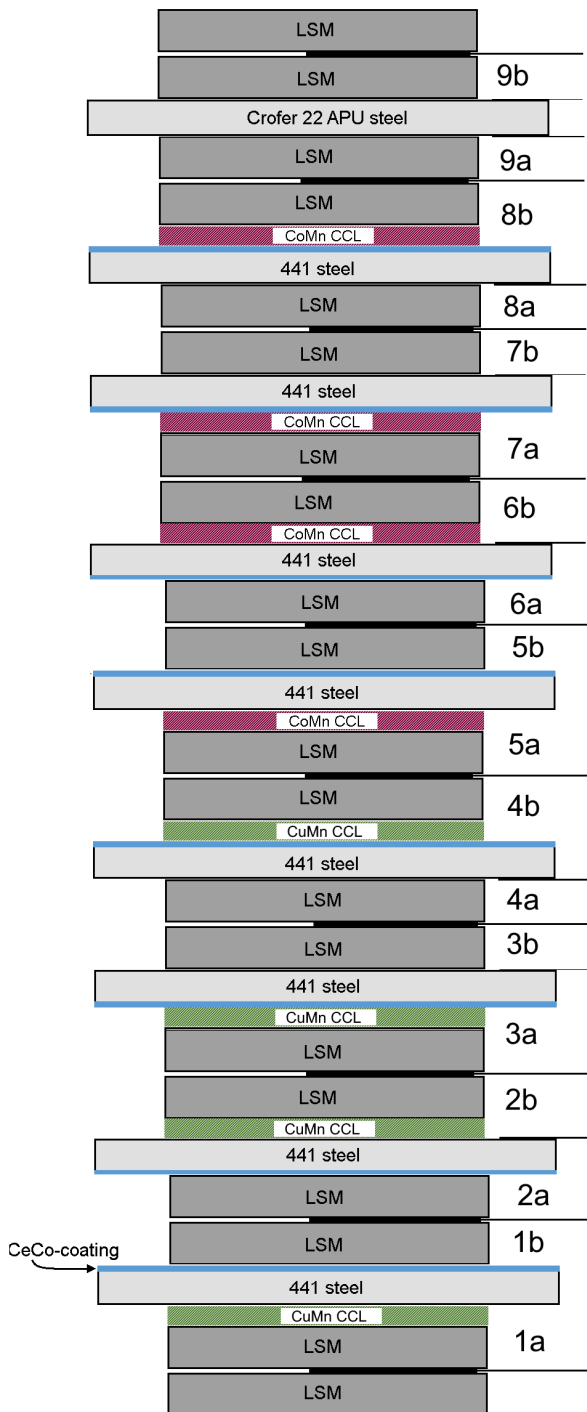
**Table 1. Overview of interfaces across which the ASR was measured. See also Figure 3.**

| Interface | 750 °C | 850 °C |
|---|---|---|
| LSM | X | X |
| 441/LSM | X | |
| 441/CeCo/LSM | X | X |
| 441/CeCo/Mn-Co/LSM | X | X |
| 441/CeCo/Mn-Cu/LSM | X | X |
| 441/Mn-Co/LSM | X | |
| 441/Mn-Cu/LSM | X | |

At least two interfaces of the same type were evaluated. After 3000 h of aging at 750 °C, the stack was thermally cycled 50 times between 750 °C and 200 °C (120 °C/h heating and cooling rate), with a dwell of 5 h at 750 °C between each thermal cycle. The stack aged at 850 °C was cooled down after nearly 3000 h of aging and will be tested for thermal cycling at a later point.

Microstructural characterization after the ASR measurement at 750 °C was performed using a scanning electron microscope (SEM, Zeiss Merlin) equipped with an energy dispersive X-ray spectrometer (EDS, Bruker). For this purpose, the whole ASR stack was embedded in epoxy and polished using SiC paper and diamonds in suspension in order to reveal the cross section. All EDS spectra were collected at an acceleration voltage of 15 kV. Microstructural characterization after the ASR measurement at 850 °C will be completed once the thermal cycles are performed.
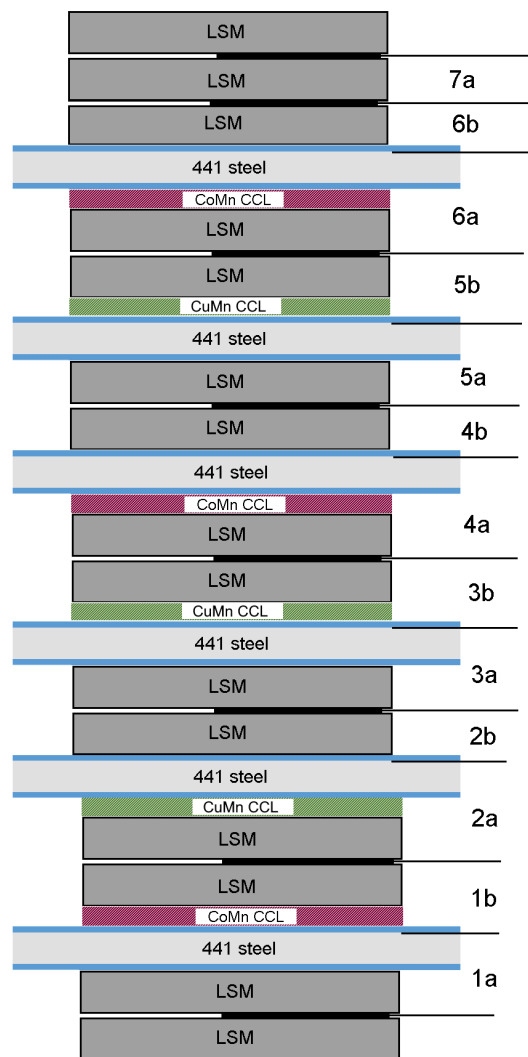
**Figure 3: Set-up for measuring the area specific resistance (a) at 750 °C, (b) at 850 °C.**

# 3 Results and discussion

## 3.1 Area specific resistance at 750 °C

The ASR measured across the different interfaces during isothermal aging at 750 °C in air is shown in Figure 4. For clarity, only one curve representative for each interface is plotted. The maximum difference between two ASR measurements of the same interface was ±3 m$\Omega$cm$^2$ for all but the 441/LSM interfaces, for which the scatter was greater (±16 m$\Omega$cm$^2$). An overview of the average ASR values measured at the start of the test and after 3000 h of aging is given in Table 1. During the 3000 h period the samples were exposed to two unplanned thermal cycles (at ca. 400 h and 2100 h), but this did not influence the results significantly.

Note that the ASR is calculated on the basis of the nominal contact area (4 cm$^2$), and that there likely is some difference in the actual contact area among the different samples, e.g. due to slight misalignment between the components and other unintended differences in the established area of contact. For this reason, the change in ASR with time provides a more important measure for comparison than the absolute values of the ASR. A degradation rate (increase in ASR with time) was calculated by a linear fit of the ASR recorded the last 500 h of isothermal aging. The results are presented in Table 1.

For all but the 441/LSM interfaces the ASR decreased during the initial 1000-2000 h of aging due to improvement of the area of contact and improved conductance of the green and only mildly sintered layers. The is primarily related to creep and sintering of the LSM contacting plates, which are pre-sintered under mild conditions and coated with a LSM/Co$_2$O$_3$ layer. As seen in Figure 4, the ASR measured across a single LSM plate continues to decrease over the entire duration of the measurement.

The ASR of the 441/LSM interface increased rapidly from the start of the measurement and reached 70±16 m$\Omega$cm$^2$ after 3000 h of aging. The high ASR can be attributed to the relatively faster growth of poorly conductive oxide scales (Cr$_2$O$_3$ and SiO$_2$) on the uncoated 441 steel. Compared to the uncoated steel, the ASR after 3000 h of aging is reduced by a factor of 2.6 with the CeCo coating. The low and stable ASR for the 441/CeCo/LSM interface indicates a reduced growth rate and/or improved electrical conductivity of the oxide scale.

Comparing the ASR measured for an interface *with* the contact layer (e.g. 441/CeCo/Mn-Co/LSM) with the equivalent interface *without* the contact layer (e.g. 441/CeCo/LSM), it is clear that the contact layer does not contribute significantly to the cross-plane resistance. This is reasonable considering the much higher electrical conductivity (at 750 °C) of MnCo$_2$O$_4$ (70 S/cm) [2] and Cu$_{1.3}$Mn$_{1.7}$O$_4$ (225 S/cm) [1] compared to Cr$_2$O$_3$ (0.1-0.01 S/cm [6,7]) and SiO$_2$ (10$^{-10}$-10$^{-8}$ S/cm [8]), which are the primary constituents of the oxide scale formed on the 441 steel. The contact layers may nevertheless indirectly have influence on the ASR through reactions with the coating, oxide scale and/or LSM plates.

According to the degradation rates presented in Table 1, the Mn-Cu contact layer results in a small improvement compared to the CeCo coating alone, while the Mn-Co contact layer slightly increases the degradation rate relative to the 441/CeCo/LSM interface.

Applying the Mn-Co or Mn-Cu contact layers directly to the 441 (i.e. no CeCo coating) also results in low and more stable ASR compared to the bare steel. This is not surprising considering that the oxidized form of the contact layers, i.e. $MnCo_2O_4$ and $Cu_{1.3}Mn_{1.7}O_4$, have been employed as interconnect coatings [4,9,10]. Nevertheless, it is clear that the best performance in terms of ASR is achieved by combining the contact layer with a CeCo coating. The CeCo coating is furthermore beneficial for reducing the release of poisonous Cr(VI)-species from the interconnect, as demonstrated in previous work [11].
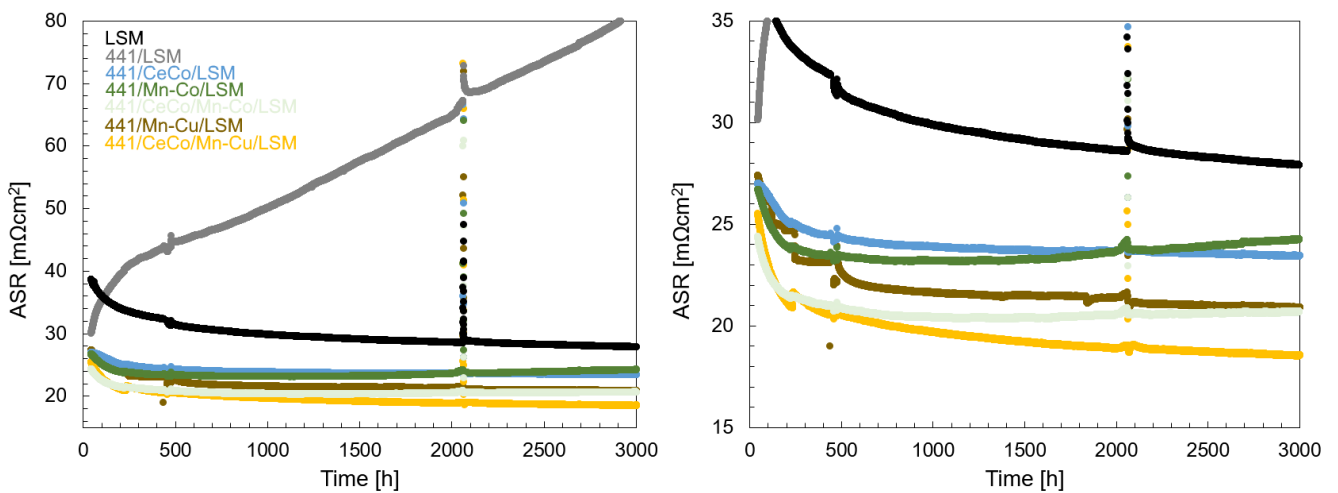


**Figure 4: ASR measured in air at 750 °C. Right side plot shows an excerpt of the ASR between 15 and 35 mΩcm².**

**Table 2. ASR measured initially and after 3000 h at 750 °C. Degradation rates extracted from last 500 h of ASR measurement. Average and standard deviation of 2-4 interfaces of the same kind. A negative degradation rate indicates a *decreasing* ASR with time.**

| Interface | Initial ASR [mΩcm²] | ASR after 3000 h [mΩcm²] | Degr. rate [mΩcm²/1000h] |
|---|---|---|---|
| LSM | 39 | 28 | -0.7 |
| 441/LSM | 31±3 | 70±16 | 8.8 |
| 441/CeCo/LSM | 29±3 | 25±3 | -0.3 |
| 441/Mn-Co/LSM | 27±1 | 25±1 | 0.8 |
| 441/Mn-Cu/LSM | 27±1 | 21±1 | 0.3 |
| 441/CeCo/Mn-Co/LSM | 25±1 | 19±2 | 0 |
| 441/CeCo/Mn-Cu/LSM | 24±2 | 18±1 | -0.3 |

## 3.2 Area specific resistance at 850 °C

Figure 5a shows the ASR of uncoated 441 contacted to LSM measured in air at 850 °C. The measurement was terminated after 200 h due to the very rapid increase in ASR. A picture of the sample after this test is shown in Figure 5b. Severe spallation of the steel is visible in areas where it was not covered by the contact layer. From these results it may be concluded that the uncoated 441 steel is not suitable for operation at 850 °C.
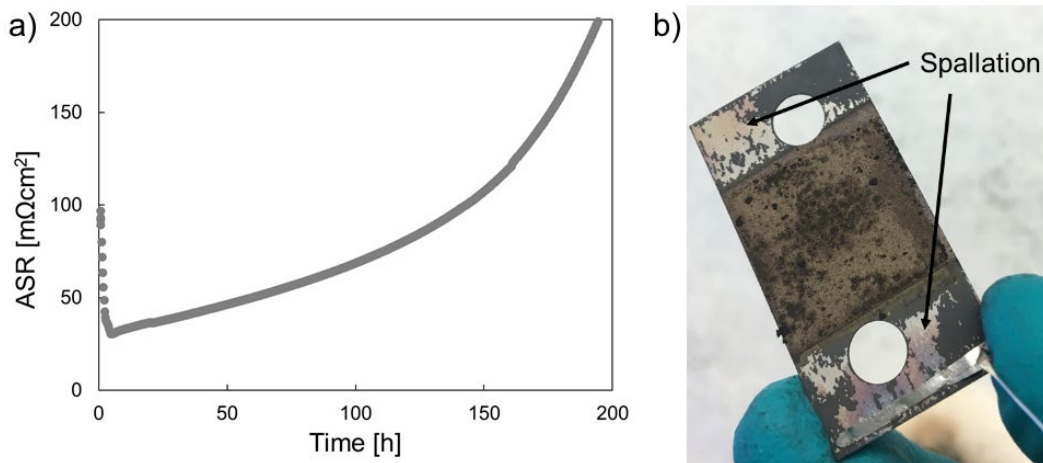


**Figure 5. (a) ASR measured for 441/LSM interface in air at 850 °C. (b) Picture of the 441 steel after 200 h aging at 850 °C.**

A new ASR measurement at 850 °C was started, this time with the steel coated with CeCo on both sides. The ASR with time is shown in Figure 6. Only one representative curve for each measurement is plotted for clarity. The stack experienced one unplanned thermal cycle (at ca. 580 h), but this did not appear to have influenced the results. During the test, the temperature decreased gradually by ca. 8 °C and after ca. 2500 h of testing became very unstable (see Figure 6). The measurement was therefore terminated after a total of 2700 h at 850 °C. Unlike with the uncoated 441 samples, the CeCo coated samples showed no visual signs of spallation at the end of the test.

The average ASR values recorded at start and the end of the measurement, and the degradation rate calculated from the slope of the curve during the last 500 h of the measurement are summarized in Table 3. The values for the 441/CeCo/LSM interface varied greatly among the six interfaces tested, as indicated by the large standard deviation. The values for the interfaces with a Mn-Co or Mn-Cu contact layer were more consistent and overall lower than for the interfaces without the contact layer. As for the measurement at lower temperature, the lowest ASR and degradation rate was measured for the interfaces with a Mn-Cu contact layer. It may also be noted that the contribution from the LSM plate is smaller at 850 °C compared to 750 °C.
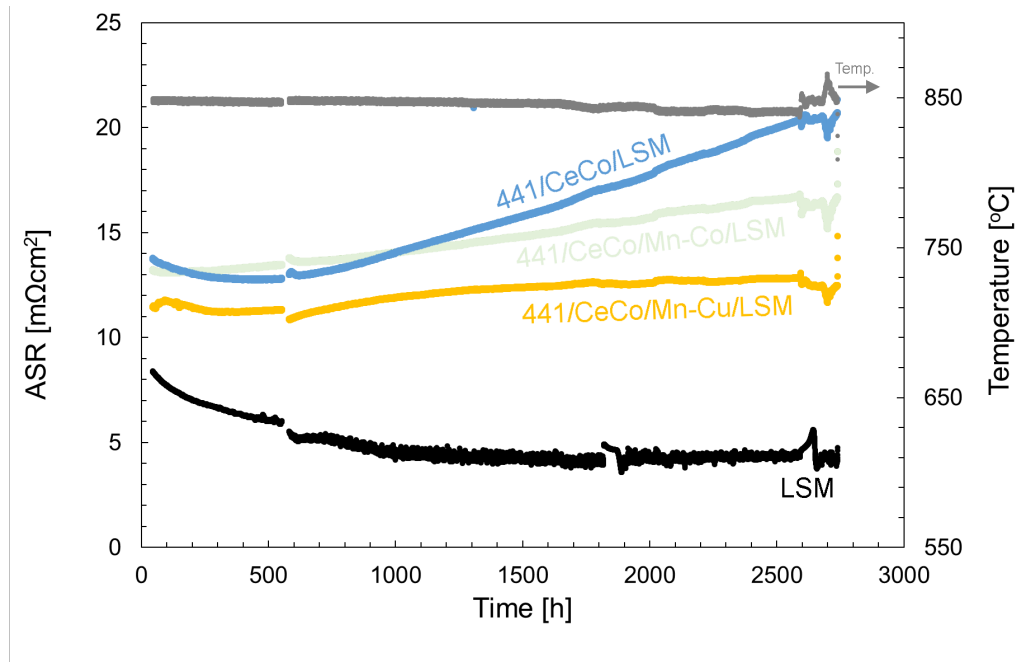
**Figure 6. ASR measured in air at 850 °C.**

**Table 3. ASR measured initially and after 2750 h at 850 °C and degradation rates extracted from last 500 h of ASR measurement. Average and standard deviation of 2-4 interfaces of the same kind. A negative degradation rate indicates a *decreasing* ASR with time.**

| Interface | Initial ASR [mΩcm²] | ASR after 2750 h [mΩcm²] | Degr. rate [mΩcm²/1000h] |
|---|---|---|---|
| LSM | 8.4 | 4.4 | 0.3 |
| 441/LSM | 31±1 | N/A | > 1000 |
| 441/CeCo/LSM | 14±1 | 25±28 | 16±22 |
| 441/CeCo/Mn-Co/LSM | 11±2 | 16±1 | 1.2±0.5 |
| 441/CeCo/Mn-Cu/LSM | 14±4 | 12±1 | -0.1±0.5 |

## 3.3 Post-test analysis 750 °C

SEM cross sectional images of selected interfaces after the ASR measurement at 750 °C are shown in Figure 7. For all of the samples, an oxide scale has formed on the steel surface after aging. On the bare 441 steel (Fig. 7a) this oxide scale consisted of an inner $Cr_2O_3$ layer and an outer $(Mn,Cr)_3O_4$ layer, according to EDS analysis. For 441 steel with a CeCo coating and/or a contact layer, the oxide scale consisted mainly of $Cr_2O_3$. A summary of the measured oxide scale thicknesses for all interfaces is given in Table 4.

For the bare 441 steel, the oxide scale was partially damaged during sample preparation (epoxy casting and polishing) due to poor adhesion of the oxide scale to the steel surface. This made it difficult to obtain an accurate measure for the oxide scale thickness. Nevertheless, the measurements in Table 4 show that the overall trend in oxide scale thickness correlates well with the ASR measurement. That is, the thinnest oxide scale was measured for the interfaces with a Mn-Cu contact layer, which also showed the lowest ASR. This further supports the conclusion that the main contribution to the ASR is the growth of the oxide scale and that the spinel oxide-forming contact layers have a sufficiently high electrical conductivity.
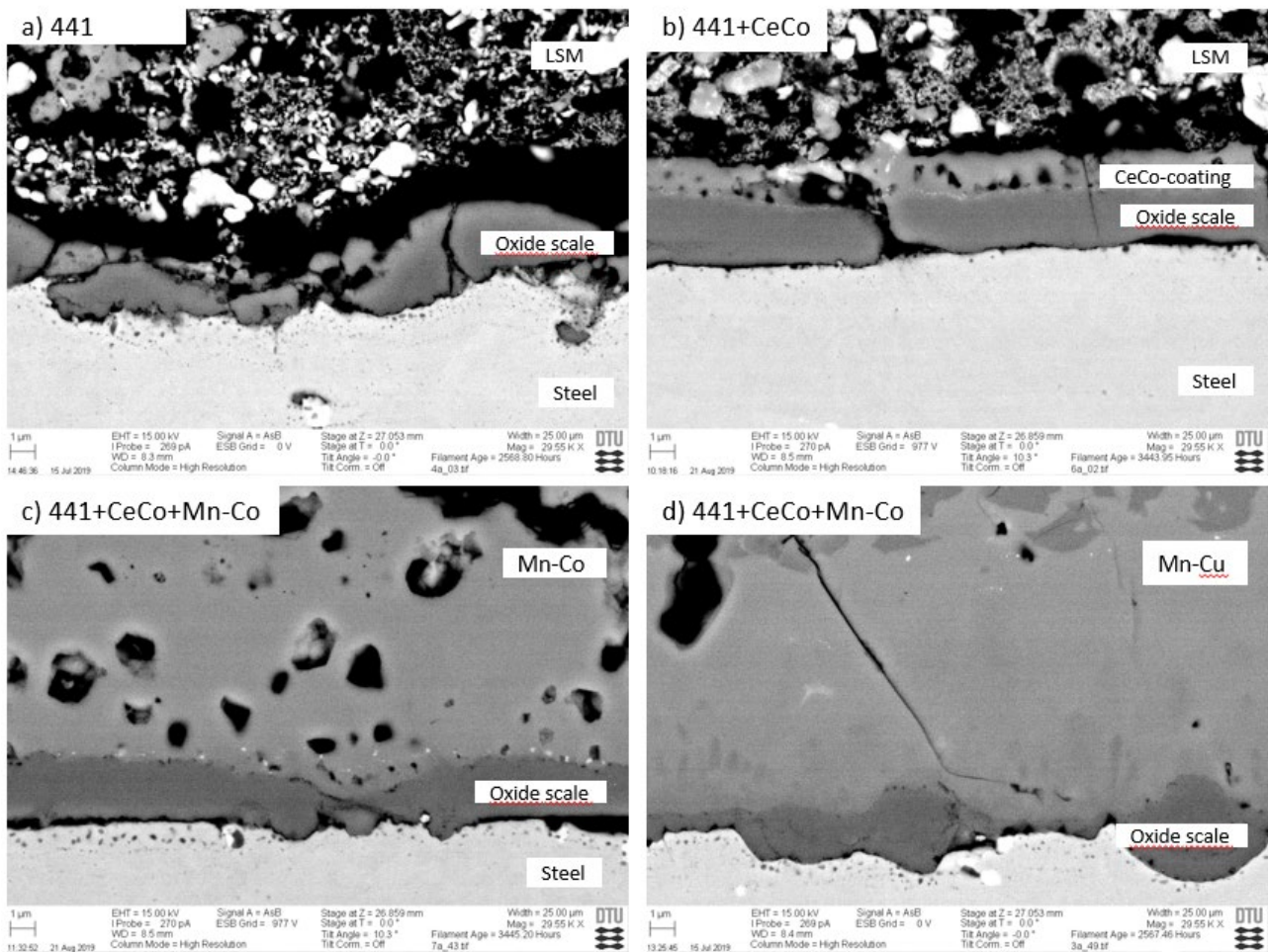


**Figure 7. SEM cross sections after ASR measurement at 750C. a) 441/LSM, b) 441/CeCo/LSM, c) 441/CeCo/Mn-Co/LSM, d) 441/CeCo/Mn-Cu/LSM.**

Figure 8 shows SEM images and EDS maps of CeCo-coated 441 samples with a Mn-Co or Mn-Cu contact layer. Both contact layers are fully oxidized after the aging at 750 °C. The Mn-Co contact layer appears to be single phase with a homogeneous composition, while the Mn-Cu contact layer clearly consist of two phases. According to quantitative EDS analysis, the composition of the two phases corresponds to $Mn_2O_3$ (purple areas) and $Mn_{1.8}Cu_{1.2}O_4$ (blue areas). These two phases are expected from the Mn-Cu-oxide phase diagram, shown in Figure 9. According to the phase

diagram, the fraction of Cu and Mn metal particles used in this work will form a spinel between 600 and 750 °C, while at lower temperature, some $Mn_2O_3$ will form in addition to the spinel oxide phase. Since the ASR samples were slowly cooled to room temperature after the long term test, it is possible that the $Mn_2O_3$ was precipitated during cooling. To confirm that a single phase spinel oxide is present at 750 °C, the sample should be quenched to room temperature.

The Co coating cannot be clearly distinguished in the EDS maps of Figure 8 due to interdiffusion with the contact layers. The Ce coating is visible as bright particles at the oxide scale/contact layer interface in case of the sample with a Mn-Co contact layer, and inside the Mn-Cu contact layer (ca. 10 μm from the oxide scale) in case of the sample with a Mn-Cu contact layer (see Fig 7c,d).

Another major difference between the two contact layers is their reactivity with the thermally grown oxide scale. For the sample with a Mn-Co contact layer, the interface between the oxide scale and the contact layer is sharp, and there is no Cr measureable in the contact layer. For the sample with a Mn-Cu contact layer the interface is more diffuse and the EDS map shows a significant amount of Cr inside the contact layer. The Cr is detected up to 16 μm from the oxide scale/contact layer interface. Table 4 gives a summary of how far away from the steel/oxide scale interface Cr was detected (by EDS linescans) for the different samples. Without any coating or contact layer (441/LSM sample), Cr diffuses far into the LSM contacting component, while both the coating and the contact layers act as effective Cr diffusion barriers. Comparing the results for CeCo coated 441 and bare 441 with a Mn-Co/Mn-Cu contact layer shows that the coating is a more efficient barrier against Cr diffusion.

Interdiffusion between the oxide scale and the contact layer is a likely reason for the thinner oxide scale measured on samples with a Mn-Cu contact layer compared to samples with a Mn-Co contact layer.
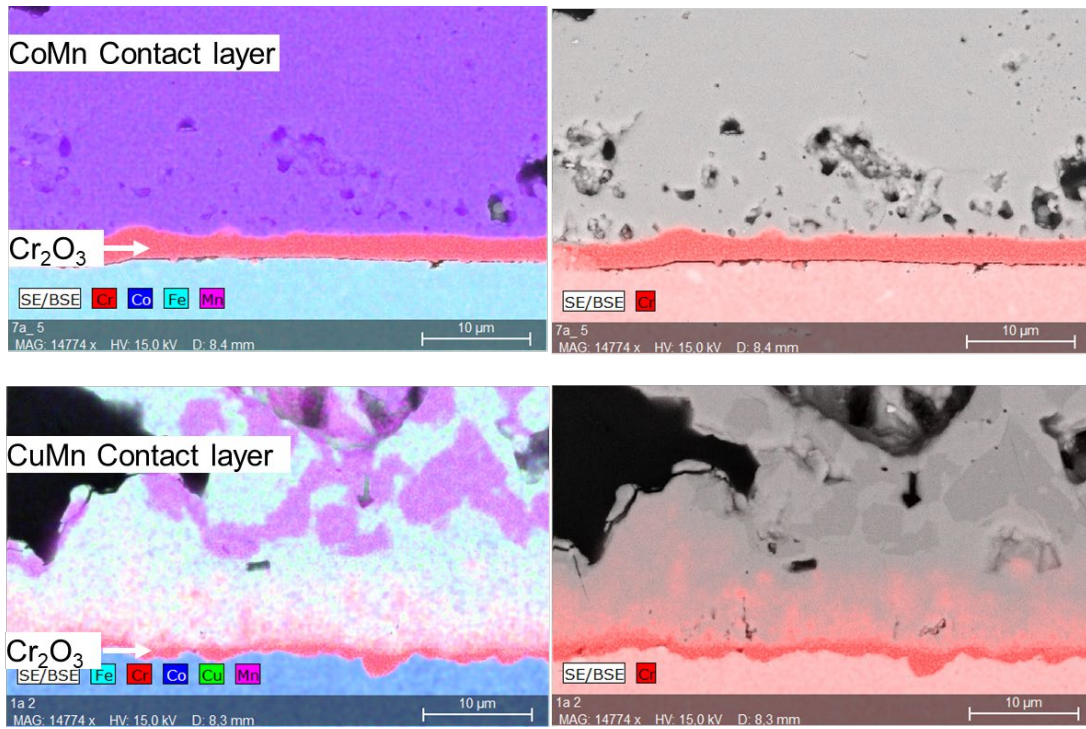
**Figure 8. SEM image overlaid with EDS maps. Top: 441/CeCo/Mn-Co/LSM interface. Bottom: 441/CeCo/Mn-Cu/LSM interface**
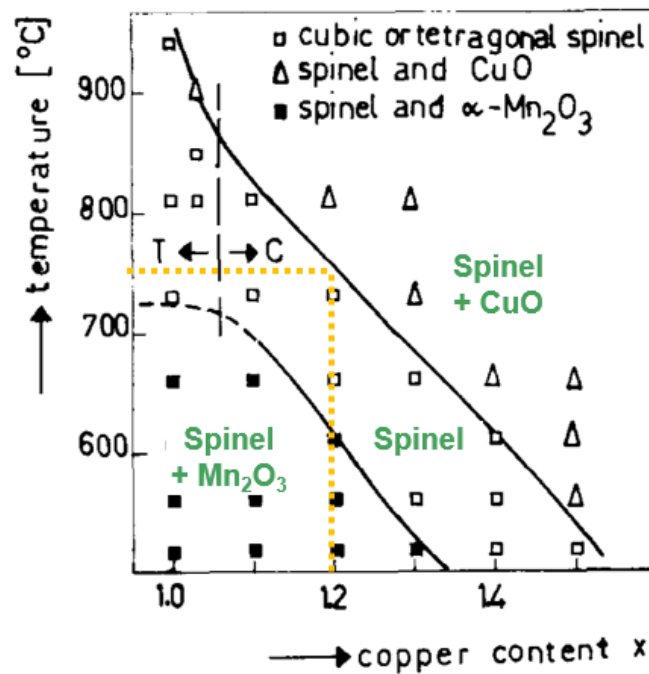


**Figure 9. MnO-CuO phase diagram from [12]. The yellow stippled lines indicate the composition and temperature used in this work.**

**Table 2. Measurement on SEM images for samples tested at 750 °C.**

| Interface | $Cr_2O_3$ thickness [μm] | Cr distance from steel surface [μm] |
|---|---|---|
| 441/LSM | 1.4* | > 52 |
| 441/CeCo/LSM | 2.1 | 3.7 |
| 441/CeCo/Mn-Co/LSM | 2.0 | 3.5 |
| 441/CeCo/Mn-Cu/LSM | 1.2 | 15 |
| 441/Mn-Co/LSM | 3.5 | 5.2 |
| 441/Mn-Cu/LSM | 1.1 | 10.5 |

*thickness measurement not reliable due to cracks/delamination of sample

# 4  Conclusions

The metallic precursors Mn-Co and Mn-Cu have been evaluated as contact materials for solid oxide cell stacks by measuring the area specific resistance (ASR) during aging at 750 °C and 850 °C. The precursors are oxidized to well-conductive spinels during aging. The ASR was found to be dominated by the oxide scale thermally grown on the 441 steel and was significantly reduced by the application of a CeCo coating. Applying the contact layers lead to a further decrease in ASR. The lowest ASR was measured for CeCo coated 441 with a Mn-Cu contact layer, at both 750 °C and 850 °C.

Post-test analysis showed that the contact layer act as a barrier against outward Cr diffusion from the steel, but that most efficient protection was achieved with the CeCo coating. The Mn-Cu contact layer increased the diffusion of Cr from the steel into the contact layer, also when the steel was coated with CeCo. This behavior may be of concern for long-term operation of stacks with the Mn-Cu contact layer, if the Cr eventually reaches the surface where it can volatilize.

# 5  Outlook

Post-test analysis of the samples tested at 850 °C is planned and will be reported in the end of the project. Furthermore, the two contact layers will be tested in the stacks of Solid Power and Sunfire.

In addition to the already planned activities, some additional experiments are recommended to further investigate the potential negative effects of Cr diffusion into the Mn-Cu contact layer:

1) There is no available information about the diffusion rate of Cr in the Mn-Cu contact layer. This may be obtained by making diffusion couples of the steel + Mn-Cu contact layer and investigating measuring the diffusion profiles after different periods of aging.
2) The volatilization of Cr from a $(Mn,Cu,Cr)_3O_4$ spinel (the reaction product formed from the oxide scale + Mn-Cu contact layer) is unknown. This may be tested by applying a thin layer of the Mn-Cu contact layer onto the CeCo coated 441 steel and aging the sample until Cr is detected on the contact layer surface. At this point, the Cr volatilization can be measured, for example by the Denuder technique at Chalmers [11].

# 6   References

[1]   A. Petric, H. Ling, Electrical Conductivity and Thermal Expansion of Spinels at Elevated Temperatures, Journal of the American Ceramic Society. 90 (2007) 1515–1520. https://doi.org/10.1111/j.1551-2916.2007.01522.x.

[2]   B. Talic, P.V. Hendriksen, K. Wiik, H.L. Lein, Thermal expansion and electrical conductivity of Fe and Cu doped MnCo2O4 spinel, Solid State Ionics. 326 (2018) 90–99. https://doi.org/10.1016/j.ssi.2018.09.018.

[3]   H.L. Frandsen, I. Ritucci, P. Khajavi, B. Talic, R. Kiebach, P.V. Hendriksen, Enhancing the Robustness of Brittle Solid Oxide Cell Stack Components, ECS Trans. 91 (2019) 2201–2211. https://doi.org/10.1149/09101.2201ecst.

[4]   B. Talic, S. Molin, K. Wiik, P.V. Hendriksen, H.L. Lein, Comparison of iron and copper doped manganese cobalt spinel oxides as protective coatings for solid oxide fuel cell interconnects, Journal of Power Sources. 372 (2017) 145–156. https://doi.org/10.1016/j.jpowsour.2017.10.060.

[5]   S. Molin, P. Jasinski, L. Mikkelsen, W. Zhang, M. Chen, P.V. Hendriksen, Low temperature processed $MnCo_2O_4$ and $MnCo_{1.8}Fe_{0.2}O_4$ as effective protective coatings for solid oxide fuel cell interconnects at 750 °C, Journal of Power Sources. 336 (2016) 408–418. https://doi.org/10.1016/j.jpowsour.2016.11.011.

[6]   A. Holt, P. Kofstad, Electrical conductivity and defect structure of $Cr_2O_3$. II. Reduced temperatures (< 1000 °C), Solid State Ionics. 69 (1994) 137–143.

[7]   J.A. Crawford, R.W. Vest, Electrical Conductivity of Single-Crystal $Cr_2O_3$, Journal of Applied Physics. 35 (1964) 2413. https://doi.org/10.1063/1.1702871.

[8]   J.K. Srivastava, M. Prasad, J.B. Wagner, Electrical Conductivity of Silicon Dioxide Thermally Grown on Silicon, J. Electrochem. Soc. 132 (1985) 955–963. https://doi.org/10.1149/1.2113993.

[9]   J.W. Stevenson, Z.G. Yang, G.G. Xia, Z. Nie, J.D. Templeton, Long-term oxidation behavior of spinel-coated ferritic stainless steel for solid oxide fuel cell interconnect applications, Journal of Power Sources. 231 (2013) 256–263. https://doi.org/10.1016/j.jpowsour.2013.01.033.

[10]   P. Wei, M.R. Bateni, A. Petric, Conversion of copper and manganese metallic films to spinel coating, J Mater Sci. 47 (2012) 5205–5215. https://doi.org/10.1007/s10853-012-6404-4.

[11]   J. Froitzheim, S. Canovic, M. Nikumaa, R. Sachitanand, L.G. Johansson, J.E. Svensson, Long term study of Cr evaporation and high temperature corrosion behaviour of Co coated ferritic

steel for solid oxide fuel cell interconnects, Journal of Power Sources. 220 (2012) 217–227. https://doi.org/10.1016/j.jpowsour.2012.06.092.

[12]  A.D.D. Broemme, V.A.M. Brabers, Preparation and properties of copper- and manganese containing mixed oxides, Solid State Ionics. 16 (1985) 171–177. https://doi.org/10.1016/0167-2738(85)90040-2.

# 7  Acknowledgment